Interplay of multiple vibrational spectral densities in femtosecond nonlinear spectroscopy of liquids

Vadim Khidekel, Vladimir Chernyak, and Shaul Mukamel
Department of Chemistry, University of Rochester, Rochester, New York 14627

(Received 17 June 1996; accepted 5 August 1996)

The multimode Brownian oscillator model of nonlinear response functions is generalized to include a multielectronic level system interacting with several spectral densities representing solvent and vibrational coupling to electronic energies, transition dipoles, and permanent dipoles. Applications to resonant and off-resonant transient grating as well as to infrared and fifth-order Raman photon echoes illustrate how the various spectral densities may be probed separately. © *1996 American Institute of Physics.* [S0021-9606(96)51342-5]

I. INTRODUCTION

Time-resolved vibrational spectroscopy is a powerful tool for studying intermolecular and intramolecular nuclear motions in condensed phases. Ultrafast ~ 50 fs laser pulses are short compared with typical vibrational periods, and can excite nuclear motions in liquids impulsively. This makes it possible to directly probe static and dynamic properties of local structures.

The simplest nonlinear optical techniques used to investigate molecular motions in liquids are the optical Kerr[1,2] and transient grating.[3,4] Both methods are one-dimensional: The signal depends on a single time variable, the time delay between pulses. As a result, these techniques cannot distinguish between contributions to line broadening coming from slow molecular dynamics (static, inhomogeneous broadening), or from fast relaxation processes (homogeneous broadening).[5] A deeper microscopic insight into the structure and dynamics of liquids can be achieved by multidimensional techniques, in which independent control over several time intervals is maintained.[5–7] These methods closely resemble their nuclear magnetic resonance counterparts.[8]

The lowest nonlinear response in isotropic media involves three field-matter interactions (four-wave mixing). Photon echo[9–14] and hole-burning[15–17] techniques eliminate the inhomogeneous broadening (slow and static components), and reveal dynamic information hidden underneath the broad envelopes typical for linear absorption spectra. This is possible only when the system has well separated time scales, and inhomogeneous contributions dominate the linewidth.

The multimode Brownian oscillator model provides a convenient framework for analyzing a broad class of nonlinear spectroscopic measurements.[18] In this model, nuclear motions are represented using a continuous distribution of harmonic degrees of freedom, which may be grouped into a few collective Brownian oscillator coordinates. Explicit expressions for the nonlinear response functions calculated within this model were given in two limiting cases. The first is a model of a two-level chromophore when the nuclear coordinates couple to the electronic energies (diagonal coupling), and the dipole operator is assumed independent of nuclear motions (the Condon approximation). This model has been successfully applied to electronically resonant techniques such as pump-probe, transient grating, and three-pulse photon echo.[19]

Another limit of the model was applied to electronically off-resonant measurements such as fifth- and seventh-order Raman experiments.[10,20–22] Here the coupling of nuclear coordinates to electronic energies makes a negligible contribution to the response functions, and the dominant coupling is through the dipole moment (non-Condon coupling).[6,7]

The contribution of non-Condon terms becomes dominant at off-resonant detunings.[18,23] The leading term in the signal is produced by the nonlinear dependence of the electronic polarizability on molecular vibrations.[6,7] A theoretical description of off-resonant response that takes into account the electronic polarizability dependence on nuclear degrees of freedom was presented in Refs. 6 and 24.

In this paper we derive new expressions for the nonlinear response functions using the Brownian oscillator model. We recover the existing expressions as limiting cases and generalize them in several ways. First, we go beyond the two-electronic level model to include an arbitrary number of electronic levels. Second, we incorporate transition as well as permanent dipole moments. The role of the permanent dipole is important in measurements such as electroabsorption.[25,26] Third, we allow coupling of nuclear degrees of freedom through electronic energies as well as through the dipole moments. In addition, we adopt a more compact bookkeeping which allows us to represent all Liouville-space paths using a single Hilbert-space correlation function of dipole operators.

In general, the signal depends on several spectral densities representing the coupling of nuclear degrees of freedom to transition dipoles, permanent dipoles, and electronic frequencies. The analysis of experiments is complicated by the interplay of these spectral densities. We propose experimental setups in which one of these spectral densities dominates the response so that the various contributions may be sorted out. Optical signals decrease as the external fields are tuned off resonance with respect to the electronic frequencies of the system, in a manner that is different for contributions coming from the various spectral densities. We show that it is possible to pinpoint the signatures of different spectral densities by studying the variation of the heterodyne-de-

tected transient grating (HDTG) signal with detuning. We also study the effect of the relative phase φ between the heterodyne and the probe fields. The different scaling of the $\varphi=0$ (dichroism) and $\varphi=\pi/2$ (birefringence) signals with detuning is calculated. Finally, we discuss the close formal connection between $(2n+1)$th-order off-resonant (Raman) optical response and nth-order resonant infrared signals.[27] Both are given by a formally identical combination of $(n+1)$-point correlation functions. The only difference is that the electronic polarizability (Raman), appearing in these correlation functions, should be replaced by the permanent dipole (infrared).

In Sec. II we introduce the model and express the linear response in terms of a two-point dipole correlation function. (This is generalized in Appendix A to nonlinear response of arbitrary order.) We then express the two-point dipole correlation function in terms of the four relevant nuclear spectral densities. In Sec. III we calculate the dipole correlation functions for the second- and third-order response, where additional spectral densities become relevant. In Sec. IV we apply these results to heterodyne-detected transient grating. We further analyze the effects of using polarized light, and establish the connection to dichroism and birefringence spectroscopies. Finally, in Sec. V we calculate the fifth-order off-resonant Raman signal for a two-electronic level system. We demonstrate how the nature of the signal changes as the optical frequency is tuned across an electronic transition, since different spectral densities dominate at various detunings. We further show how additional information about the signal can be obtained by using a mixed time-frequency detection.

II. LINEAR RESPONSE AND NUCLEAR SPECTRAL DENSITIES

We consider a multi-electronic level solute in a solvent described by the Hamiltonian

$$\hat{H}=\sum_j |j\rangle\hat{H}_j(\hat{\mathbf{p}},\hat{\mathbf{q}})\langle j|-\hat{V}(\hat{\mathbf{q}})E(t). \tag{2.1}$$

Here, $\hat{H}_j$ is the adiabatic Hamiltonian for the jth electronic level, and $\hat{\mathbf{p}}$ and $\hat{\mathbf{q}}$ denote nuclear momenta and coordinates. We represent the molecular and solvent nuclear degrees of freedom by a continuous distribution of harmonic coordinates.[28–32] We thus have

$$\hat{H}_j(\hat{\mathbf{p}},\hat{\mathbf{q}})=\hbar\Omega_j^0+\sum_n \frac{\hbar\omega_n}{2}[\hat{p}_n^2+(\hat{q}_n+d_{nj})^2]. \tag{2.2}$$

Here, $\hbar\Omega_j^0$ is the energy of the jth excited electronic state ($j=0$ is the ground state, and we set $\Omega_0^0\equiv 0$), $\hat{q}_n$ and $\hat{p}_n$ are the dimensionless coordinate and momentum of the nth nuclear oscillator with the frequency ω_n, and d_{nj} is the dimensionless coupling coefficient of the electronic and nuclear degrees of freedom (by definition, $d_{n0}\equiv 0$). The second term in Eq. (2.1) represents the interaction with an external electric field $E(t)$. The molecule is assumed to have both permanent (M) and transition (D) dipoles, and the dipole operator $\hat{V}$ is given by

$$\hat{V}(\hat{\mathbf{q}})=\sum_j |j\rangle\hat{M}_j(\hat{\mathbf{q}})\langle j|+\sum_{jk}[|j\rangle\hat{D}_{jk}(\hat{\mathbf{q}})\langle k|+|k\rangle\hat{D}_{jk}^{\dagger}(\hat{\mathbf{q}})\langle j|]. \tag{2.3}$$

We assume that the dipole operators depend exponentially on nuclear coordinates

$$\hat{D}_{jk}(\mathbf{q})=D_{jk}\ \exp\left\{\sum_n \omega_n\delta_n\hat{q}_n\right\}, \tag{2.4}$$

$$\hat{M}_j(\mathbf{q})=M_j\ \exp\left\{\sum_n \omega_n\mu_n\hat{q}_n\right\}, \tag{2.5}$$

where the coefficients μ_n and δ_n do not depend on the electronic levels. The factors ω_n in Eqs. (2.4) and (2.5) allow a compact notation for the spectral densities to be introduced below. Consequently, μ_n and δ_n have the units of time.

The spectral density function was originally introduced for a two-electronic level system coupled to harmonic vibrations within the Condon approximation.[18] Since we now consider a multitude of electronic levels and take into account non-Condon effects, we need to define several types of spectral densities,

$$C''_{\nu\nu'}(\omega)=\sum_n \nu_n\nu'_n\omega_n^2[\delta(\omega-\omega_n)-\delta(\omega+\omega_n)],$$

$$\nu_n,\nu'_n\equiv d_{nj},\mu_n,\delta_n. \tag{2.6}$$

These represent all pairs of d_j, δ, and μ, where j runs over the electronic levels. The optical response functions will be expressed in terms of the functions

$$g_{dd}(t)=\int_0^\infty \frac{d\omega}{\omega^2}C''_{dd}(\omega)[\coth(\beta\hbar\omega/2)(1-\cos\omega t)+i\sin\omega t-i\omega t], \tag{2.7}$$

$$\dot{g}_{d\nu}(t)=\int_0^\infty \frac{d\omega}{\omega}C''_{d\nu}(\omega)[\coth(\beta\hbar\omega/2)\sin\omega t+i(\cos\omega t-1), \tag{2.8}$$

$$\ddot{g}_{\nu\nu}(t)=\int_0^\infty d\omega C''_{\nu\nu}(\omega)[\coth(\beta\hbar\omega/2)\cos\omega t-i\sin\omega t], \tag{2.9}$$

$$\nu=\delta,\mu.$$

Here, the dot denotes a time derivative. The function $g_{\nu\nu'}(t)$ coincides with the function $g(t)$ used in the standard Brownian oscillator model [Eq. (8.25) of Ref. 18], and the functions $\dot{g}_{d\nu'}(t)$ and $\ddot{g}_{\nu\nu'}(t)$ represent additional contributions due to the dependence of the dipole operator on nuclear coordinates. Combining Eqs. (2.6) and (2.7)–(2.9), we obtain

$$g_{d_jd_j}(t)=\sum_n d_{nj}^2[\coth(\beta\hbar\omega_n/2)(1-\cos\omega_n t)+i\sin\omega_n t-i\omega_n t],$$

$$\dot{g}_{d_j\nu}(t)=\sum_n d_{nj}\nu_n\omega_n[\coth(\beta\hbar\omega_n/2)\sin\omega_n t + i(\cos\omega t-1)],$$

$$\ddot{g}_{\nu\nu}(t)=\sum_n \nu_n\nu_n\omega_n^2[\coth(\beta\hbar\omega_n/2)\cos\omega_n t - i\sin\omega_n t],$$

$$\nu_n=\delta_n,\mu_n.$$

The linear response is expressed in terms of the two-point correlation function of the dipole operator (see Appendix A)

$$P^{(1)}(t)=\frac{i}{\hbar}\int_0^\infty ds F^{(2)}(t,t-s)E(\mathbf{r},t-s)+\text{c.c.}, \qquad (2.10)$$

where

$$F^{(2)}(t,t-s)=\langle V(t)V(t-s)\rangle. \qquad (2.11)$$

We assume that initially the system is in its ground electronic state. Since only terms with even number of interactions with the transition dipole operator contribute to the trace, we have two possibilities: Both interactions are either with the permanent or the transition dipole operator. The corresponding contributions to the correlation function, denoted $F^{(2)}_{\rm MM}$ and $F^{(2)}_{\rm DD}$, may be calculated using an expansion in coherent states as outlined below. The correlation function (2.11) can be written as

$$F^{(2)}(\tau_1,\tau_2)=\mathrm{Tr}\{V(\tau_1)V(\tau_2)\rho_0\},$$

where $\rho_0=e^{-\beta H_0}/\mathrm{Tr}(e^{-\beta H_0})$ is the equilibrium density matrix. We calculate this trace using the basis set of coherent states $|z\rangle$,[33,34] defined by

$$|z\rangle=e^{za^+}|\Omega\rangle,$$

where z is a complex number, a^+ is the creation operator, and Ω denotes the ground state of the harmonic oscillator. In this basis $F^{(2)}(\tau_1,\tau_2)$ can be written as

$$F^{(2)}(\tau_1,\tau_2)=\frac{1}{\mathrm{Tr}(e^{-\beta H_0})}\int\frac{d^2z}{\langle z|z\rangle}\times\langle z|V(\tau_1)V(\tau_2)e^{-\beta H_0}|z\rangle, \qquad (2.12)$$

with

$$\mathrm{Tr}(e^{-\beta H_0})=\int\frac{d^2z}{\langle z|z\rangle}\langle z|e^{-\beta H_0}|z\rangle.$$

Since the dipole operator $V(t)$ has an exponential dependence on nuclear coordinates, we can easily calculate Eq. (2.12) by acting on the coherent state $|z\rangle$ successively by the operators $e^{-\beta H_0}$, V, the evolution operator $e^{-(i/\hbar)H_0(\tau_1-\tau_2)}$, and the second operator V. The rules for acting with exponential operators on a coherent state are summarized in Ref. 7. The resulting wave function, which retains its coherent state form at all times,

$$|z'\rangle=Ve^{-(i/\hbar)H_0(\tau_1-\tau_2)}Ve^{-\beta H_0}|z\rangle$$

is then overlapped with $\langle z|$ to calculate the trace as given by Eq. (2.12). The coherent states form an overcomplete basis set. The property that makes it particularly suitable for the present calculation is that when an exponential operator such as V acts on a coherent state, the result is also a coherent state (and not a superposition of states). This eliminates the numerous summations which appear when using the eigenstate basis and provides a compact expression for the correlation function. We thus obtain

$$F^{(2)}(\tau_1,\tau_2)=F^{(2)}_{\rm MM}(\tau_1,\tau_2)+F^{(2)}_{\rm DD}(\tau_1,\tau_2),$$

$$F^{(2)}_{\rm MM}(\tau_1,\tau_2)=M_0^2\exp\{\ddot{g}_{\mu\mu}(0)+\ddot{g}_{\mu\mu}(\tau_{21})\}, \qquad (2.13)$$

$$F^{(2)}_{\rm DD}(\tau_1,\tau_2)=\sum_j D_{j0}^2\exp\{-i\Omega_j\tau_{21}+\ddot{g}_{\delta\delta}(0)+\ddot{g}_{\delta\delta}(\tau_{21})-g_{d_jd_j}(\tau_{21})+2i\dot{g}_{\delta d_j}(\tau_{21})\}. \qquad (2.14)$$

Here, $\Omega_j\equiv\Omega_j^0+\frac{1}{2}\Sigma_j d_j^2\omega_j^2$, $\tau_{21}\equiv\tau_2-\tau_1$, and the functions $g_{\nu\nu'}(\tau)$, $\dot{g}_{\nu\nu'}(\tau)$, and $\ddot{g}_{\nu\nu'}(\tau)$ are given by Eqs. (2.7)–(2.9). Four spectral densities contribute to the response function for each electronic transition j: $g_{d_jd_j}$, which reflects the dependence of electronic transition frequency on nuclear coordinates; $\ddot{g}_{\delta\delta}$ and $\ddot{g}_{\mu\mu}$, which describes how nuclear coordinates affect the transition and permanent dipole moment; and the mixed spectral density $\dot{g}_{\delta d_j}$.

III. THE NONLINEAR RESPONSE FUNCTIONS

The nth-order nonlinear response can be expressed as a combination of the dipole correlation functions

$$F^{(n+1)}(\tau_1,\ldots,\tau_{n+1})=\langle V(\tau_1)V(\tau_2)\cdots V(\tau_{n+1})\rangle, \qquad (3.1)$$

with various permutations of the time arguments. In the standard density matrix Liouville-space formalism we maintain a complete bookkeeping of the time ordering of the various interactions. The nth-order response then contains 2^n terms.[18] In Appendix A we outline an alternative bookkeeping, which maintains only partial time ordering of the interactions with the external field (based on the Schwinger–Keldysh time loop.[35–37]) This scheme results in fewer terms and assumes a more compact form compared with the fully time-ordered density matrix formalism. It is straighforward to switch between the two pictures: By separating the various terms in Appendix A to different components, we can recover the density matrix expressions.[18] For impulsive measurements with very short pulses, the fully time ordered expressions are most appropriate, whereas when the time ordering is partially lost, e.g., by using finite and overlapping pulses, then the form given in Appendix A may be more adequate. In any event, the building blocks of both formalisms are the correlation functions (3.1), which will be evaluated below.

The second-order response is given by a three-time correlation function of dipole operators. It includes either three or one interactions with the permanent dipole operator. The corresponding contributions to the response functions will be denoted $F^{(3)}_{\rm MM}$ and $F^{(3)}_{\rm MD}$. We then have

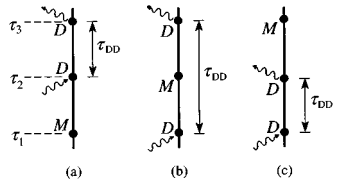

FIG. 1. All possible permutations of the permanent and transition dipole operators for the second-order response function $F^{(3)}_{\mathrm{MD}}$ [Eq. (3.3].

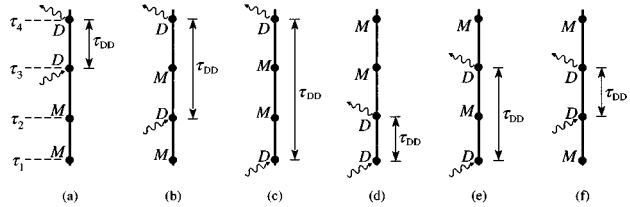

FIG. 2. All possible permutations of the permanent and transition dipole operators for the third-order response function $F^{(4)}_{\mathrm{MD}}$ [Eq. (B3)].

$$
\begin{aligned}
&F^{(3)}(\tau_1,\tau_2,\tau_3)\\
&\quad=F^{(3)}_{\mathrm{MM}}(\tau_1,\tau_2,\tau_3)+F^{(3)}_{\mathrm{MD}}(\tau_1,\tau_2,\tau_3),\\
&F^{(3)}_{\mathrm{MM}}(\tau_1,\tau_2,\tau_3)\\
&\quad=M_0^3\ \exp\{(3/2)\ddot{g}_{\mu\mu}(0)+\ddot{g}_{\mu\mu}(\tau_{21})\\
&\qquad+\ddot{g}_{\mu\mu}(\tau_{32})+\ddot{g}_{\mu\mu}(\tau_{31})\},
\end{aligned}
\tag{3.2}
$$

$$
\begin{aligned}
&F^{(3)}_{\mathrm{MD}}(\tau_1,\tau_2,\tau_3)\\
&\quad=\sum_{k=1}^{3}\sum_{j}M_k D_{j0}^2\ \exp\{-i\Omega_j\tau_{\mathrm{DD}}+\ddot{g}_{\mu\mu}(0)+\ddot{g}_{\delta\delta}(0)\\
&\qquad+\ddot{g}_{\delta\delta}(\tau_{\mathrm{DD}})-g_{d_jd_j}(\tau_{\mathrm{DD}})+2i\dot{g}_{\delta d_j}(\tau_{\mathrm{DD}})+\ddot{g}_{\delta\mu}(\tau^{(1)}_{\mathrm{MD}})\\
&\qquad+\ddot{g}_{\delta\mu}(\tau^{(2)}_{\mathrm{MD}})+i\dot{g}_{d_j\mu}(\tau^{(1)}_{\mathrm{MD}})+i\varepsilon_k\dot{g}_{d_j\mu}(\tau^{(2)}_{\mathrm{MD}})\},
\end{aligned}
\tag{3.3}
$$

Here, $\tau_{ij}\equiv\tau_i-\tau_j$, $i,j=1,2,3$, and the time variables τ_{DD} and τ_{MD} in (3.3) denote the intervals between the two D-interactions and between the D- and M-interactions, respectively. The k summation in Eq. (3.3) represents the three possible choices of the interval τ_{DD}: $\tau_2-\tau_1$, $\tau_3-\tau_2$, and $\tau_3-\tau_1$; these choices are depicted in Figs. 1(a)–1(c). The subscript k of M_k denotes whether the ground- or excited-state permanent dipole operator is involved. This also determines the parameter ε_k. The time intervals and the parameters used in Eq. (3.3) are listed in Table I.

The third order response involves four interactions with the dipole operator; in this case there are three possibilities corresponding to 4, 2, or 0 interactions with the permanent dipole operator. The last case, in turn, is divided into two: Either all four transitions involve only a single pair of electronic levels, or three levels participate, i.e., the system is excited twice and then returns to the ground state. We denote these contributions by $F^{(4)}_{\mathrm{MM}}$, $F^{(4)}_{\mathrm{MD}}$, $F^{(4)}_{\mathrm{DD}}$, and $F^{(4)}_{\mathrm{DD}'}$ respectively. They are given in Appendix B [Eqs. (B1)–(B5)], and all relevant permutations of transition and permanent dipoles for $F^{(4)}_{\mathrm{MD}}$ are given in Fig. 2.

TABLE I. The parameters corresponding to three terms of the sum $F^{(3)}_{\mathrm{MD}}$ [Eq. (3.3), the diagrams (a)–(c) in Fig. 1].

k	Diagram	τ_{DD}	$\tau^{(1)}_{\mathrm{MD}}$	$\tau^{(2)}_{\mathrm{MD}}$	ε_k	M_k
1	(a)	τ_{32}	τ_{31}	τ_{21}	-1	M_0
2	(b)	τ_{21}	τ_{31}	τ_{32}	-1	M_0
3	(c)	τ_{31}	τ_{21}	τ_{32}	1	M_j

IV. HETERODYNE-DETECTED TRANSIENT GRATING; NON-CONDON EFFECTS IN BIREFRINGENCE AND DICHROISM

In this section we show how to distinguish experimentally between the contributions of spectral densities related to different types of coupling of electronic and nuclear degrees of freedom. We consider a two-electronic level solute with the Hamiltonian given by Eq. (2.2) with $j=1$. We neglect the permanent dipole, and non-Condon effects are incorporated through the dependence of the transition dipole operator on nuclear coordinates [Eq. (2.4)].

We start with the normalized linear absorption line shape,

$$
\sigma_a(\omega)=\frac{1}{\pi\hbar}\ \mathrm{Re}\int_0^\infty F^{(2)}_{\mathrm{DD}}(t,0)e^{i\omega t}dt, \tag{4.1}
$$

where $F^{(2)}_{\mathrm{DD}}$ is given by Eq. (2.14). Neglecting the mixed spectral density $C''_{d\delta}(\omega)=0$, Eq. (2.14) becomes

$$
F^{(2)}_{\mathrm{DD}}(t,0)=D^2\ \exp\{-i\Omega t+\ddot{g}_{\delta\delta}(0)+\ddot{g}_{\delta\delta}(t)-g_{dd}(t)\}. \tag{4.2}
$$

The time dependence of this correlation function is governed by the following combination of the two spectral densities: $\ddot{g}_{\delta\delta}(t)-g_{dd}(t)$, and we cannot therefore differentiate between the two. We assume that both spectral densities represent a single overdamped Brownian oscillator,

$$
C''_{dd}(\omega)=2\lambda_d\frac{\omega\Lambda_d}{\omega^2+\Lambda_d},\quad C''_{\delta\delta}(\omega)=2\lambda_\delta\frac{\omega\Lambda_\delta}{\omega^2+\Lambda_\delta^2}. \tag{4.3}
$$

Note that the coupling parameters λ_d and λ_δ have the units of frequency and time respectively. Using Eqs. (2.7)–(2.9), we obtain in the high-temperature limit $\beta\hbar\Lambda\ll1$,

$$
\begin{aligned}
g_{dd}(t)&=\frac{\lambda_d}{\Lambda_d}\left(\frac{2}{\beta\hbar\Lambda_d}[e^{-\Lambda_d|t|}+\Lambda_d|t|-1]\right.\\
&\qquad\left.-i\ \mathrm{sign}\ t[e^{-\Lambda_d|t|}-1]\right),\\
\ddot{g}_{\delta\delta}(t)&=\Lambda_\delta\lambda_\delta\left(\frac{2}{\beta\hbar\Lambda_\delta}-i\ \mathrm{sign}\ t\right)e^{-\Lambda_\delta|t|}.
\end{aligned}
$$

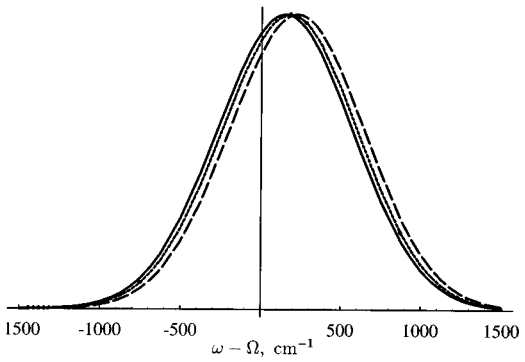

FIG. 3. Linear absorption spectrum for a two-level system. Solid line: The Condon limit $\lambda_\delta=0$; dotted line: $\lambda_\delta=0.2$ ps, dashed line: $\lambda_\delta=0.5$ ps. For other parameters see the text.

In Fig. 3 we show the absorption line shape for this model. We use the following parameters for the Brownian oscillator spectral densities: $\Lambda_d=\Lambda_\delta=0.5$ ps^{-1}, $\lambda_d=2.5$ ps^{-1}, $\beta\hbar\Lambda_j=0.025$. The parameter λ_δ reflects the strength on the non-Condon effects; $\lambda_\delta=0$ corresponds to the Condon limit, in which the dipole operator does not depend on nuclear coordinates (solid line), and the dotted and dashed lines are calculated for $\lambda_\delta=0.2$ ps and $\lambda_\delta=0.5$ ps, respectively. For these parameters, the spectral density $C''_{\delta\delta}(\omega)$, associated with the coupling between the dipole operator and nuclear coordinates, hardly affects the line shape: it only produces a small shift without changing its profile. We therefore cannot infer from linear measurements whether non-Condon effects are important and what is the origin of the line broadening.

To differentiate between the two contributions, we will consider the heterodyne-detected transient grating (HDTG), and show how the presence of the spectral density $C''_{\delta\delta}(\omega)$ can be easily established experimentally. This technique can therefore be used to identify whether the line broadening comes from the coupling between the electronic and nuclear degrees of freedom, or from the dependence of the dipole operator on nuclear degrees of freedom.

In the HDTG technique, the system is subjected to two pump pulses propagating in the directions $\mathbf{k}_1$ and $\mathbf{k}_2$. These pulses create a transient grating in the medium. The probe pulse (with wave vector $\mathbf{k}_3$) then undergoes a Bragg diffraction, and the signal, generated in the direction $\mathbf{k}_s=\mathbf{k}_1-\mathbf{k}_2+\mathbf{k}_3$, is finally mixed with a fourth, heterodyne, field with frequency ω_h and phase φ relative to the probe pulse. Hereafter we assume that both pump pulses have the same temporal envelope and frequency ω_1; the frequency of the probe and heterodyne fields is ω_2, and they too have the same envelope. We denote the delay between the probe pulse and the two pump pulses by τ_0. The total field can then be written as

$$\begin{aligned}E(\mathbf{r},t)=&\mathscr{E}_1(t)e^{i\mathbf{k}_1\mathbf{r}-i\omega_1 t}+\mathscr{E}_1(t)e^{i\mathbf{k}_2\mathbf{r}-i\omega_1 t}\\&+\mathscr{E}_2(t-\tau_0)e^{i\mathbf{k}_3\mathbf{r}-i\omega_2 t}\\&+\mathscr{E}_2(t-\tau_0)e^{i\mathbf{k}_s\mathbf{r}-i\omega_2 t+i\varphi}+\text{c.c.}\end{aligned}\tag{4.4}$$

The transient grating signal is given by[18]

$$S(\omega_1,\omega_2;\tau_0)=-2\,\mathrm{Im}\int_{-\infty}^{\infty}e^{i\varphi}\mathscr{E}_2^*(t)P^{(3)}(\mathbf{k}_s,t)dt.\tag{4.5}$$

In Appendix C we calculate the HDTG signal assuming pulses short compared with the nuclear dynamics but long compared with the electronic dephasing timescale (this is known as the snapshot limit).[18] We express the signal in terms of the four-point correlation function $F^{(4)}_{\mathrm{DD}}$ [Eq. (B4)], which is factorized into a fast-oscillating term $\exp\{-i\Omega(t_4-t_3+t_2-t_1)\}$ and a slowly-varying function $\Phi(t_1,t_2,t_3,t_4)$,

$$F^{(4)}_{\mathrm{DD}}(t_1,t_2,t_3,t_4)\equiv D^4e^{-i\Omega(t_4-t_3+t_2-t_1)}\Phi(t_1,t_2,t_3,t_4).\tag{4.6}$$

In the rotating-wave approximation, which holds when the detunings $\omega_j-\Omega$ are much smaller than the optical frequencies, we obtain

$$\begin{aligned}S(\omega_1,\omega_2;\tau_0)=&\frac{2}{\hbar^3}E_1E_2\,\mathrm{Re}\iint_0^\infty e^{i\varphi}d\tau_1d\tau_2\{e^{i(\omega_1-\Omega)\tau_1}e^{-i(\omega_2-\Omega)\tau_2}[\Phi(-\tau_1,0,\tau_0,\tau_{02})-\Phi(-\tau_1,\tau_0,\tau_{02},0)]\\&+e^{-i(\omega_1-\Omega)\tau_1}e^{-i(\omega_2-\Omega)\tau_2}[\Phi(0,\tau_0,\tau_{02},-\tau_1)-[\Phi(\tau_0,\tau_{02},0,-\tau_1)\},\end{aligned}\tag{4.7}$$

where we used the notation $\tau_{02}\equiv\tau_0-\tau_2$.

In the following calculations we assume that all laser pulses have the same frequency, $\omega_1=\omega_2\equiv\omega$, and calculate the signal (C4) for the model used in Fig. 3. We shall be interested primarily in the dependence of this signal on detuning, because this should reveal the origin of the spectral densities. We further study how the phase φ affects the signal. In Figs. 4(a) and 4(b) we present the dichroism ($\varphi=0$) and the birefringence ($\varphi=\pi/2$) signals, respectively. The variation of the signals with the detuning of both laser pulses from the electronic transition frequency are shown. The delay between the pulses was varied from $\tau_0=0.5$ ps to $\tau_0=2$ ps.

It is clear from Fig. 4 that the HDTG signals are far more sensitive to non-Condon contributions compared with the linear absorption line shape. The same parameters that hardly produced any effect for linear absorption, considerably change the behavior of transient grating signals, making it possible to immediately recognize the signatures of the non-Condon contributions. The changes are clearly seen both for the dependence on the detuning and on the delay between

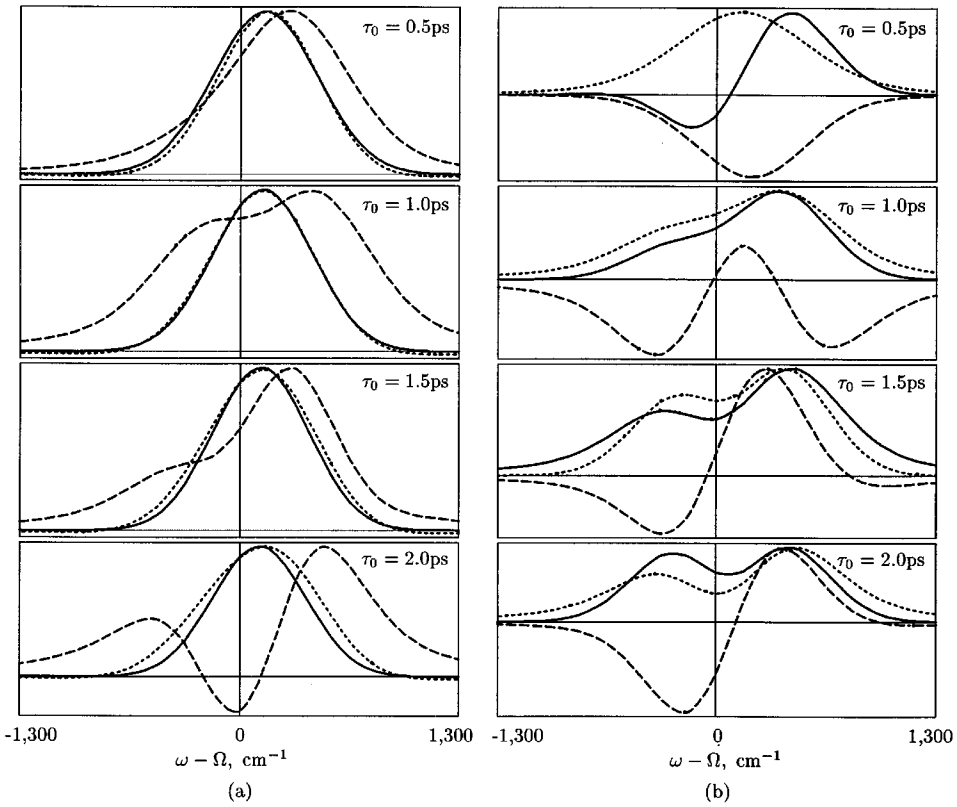

FIG. 4. The dichroism (a) and birefringence (b) signals as a function of the detuning between the laser pulses and the electronic transition frequency. The delay between the pulses is shown on each panel. The parameters of the Brownian oscillator model used are the same as in Fig. 3. Solid line: the Condon limit ($\lambda_\delta = 0$); dotted line: $\lambda_\delta = 0.2$ ps; dashed line: $\lambda_\delta = 0.5$ ps. The curves in each panel are normalized to have the same maximum.

the pulses. These effects are especially pronounced for birefringence, which appears to be more sensitive to non-Condon effects than dichroism. The oscillatory dependence of the signal on the delay between the pulses can also serve as a test for non-Condon effects: This arises from interference between terms corresponding to different Liouville-space paths.

The signals for large detunings (compared with linewidth) are displayed in Fig. 5 for dichroism (top panel) and birefringence (bottom panel). All curves are given for the delay $\tau_0 = 1.5$ ps. The solid lines represent the Condon limit ($\lambda_\delta = 0$), the dashed lines ($\lambda_\delta = 0.5$ ps) show how the signal changes as non-Condon effects are switched on. This gives us one more way to recognize non-Condon contributions: The manner with which the signal decreases with the detuning changes drastically. In the Condon limit the line shape of an overdamped Brownian oscillator in the slow modulation limit has a Gaussian profile,[18] and we see the fast decay of solid lines in Fig. 5 (the solid curves bend down, which reflects their exponential dependence on detuning). Once we include a non-Condon coupling, the dependence switches to a power law. We can deduce from the slope of dashed lines that the signal scales approximately as $\Delta\omega^{-3}$ for dichroism, and $\Delta\omega^{-2}$ for birefringence, as predicted in Ref. 18.

V. FIFTH-ORDER RAMAN ECHO

In this section we study heterodyne-detected fifth-order Raman spectroscopic measurements, in which the system is subjected to two pairs of short laser pulses followed by a probe pulse [Fig. 6(a)]. The signal is then overlapped with the heterodyne pulse (with the frequency ω_s), and the signal is given by

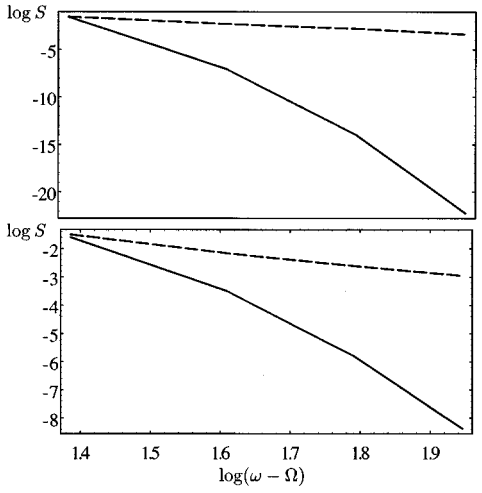

FIG. 5. The dichroism (top panel) and the birefringence (bottom panel) signals in the logarithmic scale for the detunings large compared with the linewidth. The delay between the pulses is $\tau_0 = 1.5$ ps. Solid lines represent the Condon limit ($\lambda_\delta = 0$), and the dashed lines are calculated for $\lambda_\delta = 0.5$ ps. All other parameters are the same as in Fig. 3.

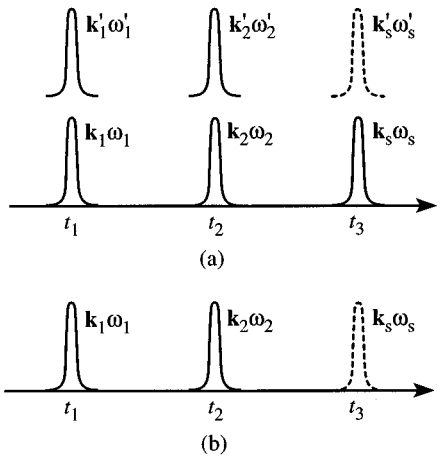

FIG. 6. Pulse configuration for (a) fifth-order Raman and (b) second-order infrared spectroscopy.

$$S=-2\,\mathrm{Im}\int_{-\infty}^{\infty}\mathscr{E}_h^*(t-t_3)\mathscr{P}^{(5)}(t)dt. \tag{5.1}$$

The fifth-order optical response function is expressed in terms of the six-point correlation function $F_{\mathrm{DD}}^{(6)}(\tau_1,\tau_2,\tau_3,\tau_4,\tau_5,\tau_6)$. Since the pulses come in pairs [Fig. 6(a)], and are assumed to be short compared with nuclear dynamics, we will be able to express the response in terms of six-point correlation function containing only three time arguments: t_1, t_2, and t_3, each taken twice. The relevant Liouville-space paths are given in Fig. 7, and the necessary six-point correlation functions corresponding to these paths are

$$F_{\mathrm{DD}}^{(6)}(t_1,t_1,t_2,t_2,t_3,t_3)=D^6\,\exp\{6\ddot{g}_{\delta\delta}(0)+4\ddot{g}_{\delta\delta}(t_{21})+4\ddot{g}_{\delta\delta}(t_{32})+4\ddot{g}_{\delta\delta}(t_{31})\},$$

$$F_{\mathrm{DD}}^{(6)}(t_1,t_1,t_3,t_3,t_2,t_2)=D^6\,\exp\{6\ddot{g}_{\delta\delta}(0)+4\ddot{g}_{\delta\delta}(t_{21})-4\ddot{g}_{\delta\delta}(t_{32})+4\ddot{g}_{\delta\delta}(t_{31})\},$$

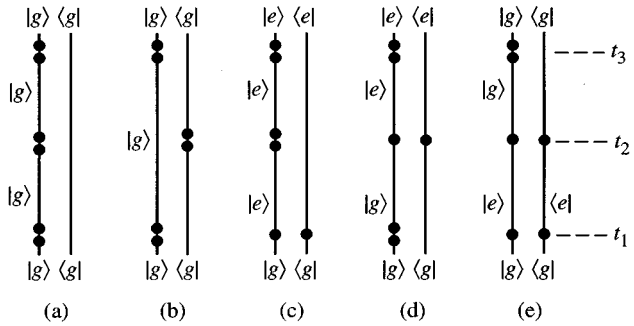

FIG. 7. The Liouville-space paths for fifth-order Raman spectroscopy.

$$F_{\mathrm{DD}}^{(6)}(t_1,t_1,t_2,t_3,t_3,t_2)=D^6\,\exp\{6\ddot{g}_{\delta\delta}(0)+4\ddot{g}_{\delta\delta}(t_{21})+4\,\mathrm{Re}\,\ddot{g}_{\delta\delta}(t_{32})+4\ddot{g}_{\delta\delta}(t_{31})-4\,\mathrm{Im}\,\dot{g}_{\delta d}(t_{21})\},$$

$$F_{\mathrm{DD}}^{(6)}(t_1,t_2,t_2,t_3,t_3,t_1)=D^6\,\exp\{6\ddot{g}_{\delta\delta}(0)+4\,\mathrm{Re}[\ddot{g}_{\delta\delta}(t_{21})-\ddot{g}_{\delta\delta}(t_{31})]-4\ddot{g}_{\delta\delta}(t_{32})-4\,\mathrm{Im}[\dot{g}_{\delta d}(t_{21})+\dot{g}_{\delta d}(t_{31})]\},$$

$$F_{\mathrm{DD}}^{(6)}(t_1,t_2,t_3,t_3,t_2,t_1)=D^6\,\exp\{6\ddot{g}_{\delta\delta}(0)+4\,\mathrm{Re}[\ddot{g}_{\delta\delta}(t_{21})+\ddot{g}_{\delta\delta}(t_{32})+\ddot{g}_{\delta\delta}(t_{31})]-4\,\mathrm{Im}[\dot{g}_{\delta d}(t_{21})-\dot{g}_{\delta d}(t_{32})+\dot{g}_{\delta d}(t_{31})]\}.$$

with $t_{ij}\equiv t_i-t_j$, $i,j=1,2,3$.

We shall now discuss the contributions of different paths (Fig. 7) to the signal (5.1), paying particular attention to the dependence on the detuning between the field and the electronic transition frequency. We start with paths (a) and (b). These paths contain no excited-state evolution periods, and in the off-resonant regime we can integrate over the time intervals during which the system is in an electronic coherence and obtain

$$S_a=\frac{1}{\hbar^5}\int_{-\infty}^{\infty}dt_3\int_{-\infty}^{t_3}dt_2\int_{-\infty}^{t_2}dt_1|\mathscr{E}(t_1)|^2|\mathscr{E}(t_2)|^2\times|\mathscr{E}(t_3)|^2F_{\mathrm{DD}}^{(6)}(t_1,t_1,t_2,t_2,t_3,t_3), \tag{5.2}$$

$$S_b=\frac{1}{\hbar^5}\int_{-\infty}^{\infty}dt_3\int_{-\infty}^{t_3}dt_2\int_{-\infty}^{t_2}dt_1|\mathscr{E}(t_1)|^2|\mathscr{E}(t_2)|^2\times|\mathscr{E}(t_3)|^2F_{\mathrm{DD}}^{(6)}(t_1,t_1,t_3,t_3,t_2,t_2), \tag{5.3}$$

where we assumed that the third pulse is the heterodyne field and $\omega_i=\omega_i'$ It was shown in Ref. 38 that in off-resonant Raman spectroscopy each pair of interactions with the transition dipole can be replaced by an effective interaction with the electronic polarizability α defined as

$$\alpha(\omega,q)\equiv[D(q)]^2\left(\frac{1}{\Omega-\omega}+\frac{1}{\Omega+\omega}\right). \tag{5.4}$$

We thus see that $F_{\mathrm{DD}}^{(6)}(t_1,t_1,t_2,t_2,t_3,t_3)$ reduces to the three-point correlation function $F_{\mathrm{MM}}^{(3)}(t_1,t_2,t_3)$ [Eq. (3.2)] provided we replace $\ddot{g}_{\delta\delta}$ by $\ddot{g}_{\mu\mu}/4$ and change in the latter μ for α as defined in (5.4). Clearly, as we tune the frequency off resonance, S_a and S_b scale as $(\Omega-\omega)^{-3}$.

Consider now the scaling of path (e) whose contribution to the signal is given by

$$S_e=\frac{1}{\hbar^5}\int_{-\infty}^{\infty}dt_3\int_{-\infty}^{t_3}dt_2\int_{-\infty}^{t_2}dt_1\int_{-\infty}^{t_3}dt_3'\int_{-\infty}^{t_3'}dt_2'\int_{-\infty}^{t_2'}dt_1'\times\mathscr{E}(t_3)\mathscr{E}(t_2)\mathscr{E}(t_1)\mathscr{E}^*(t_3')\mathscr{E}^*(t_2')\mathscr{E}^*(t_1')\times F_{\mathrm{DD}}^{(6)}(t_1,t_2,t_3,t_3',t_2',t_1'). \tag{5.5}$$

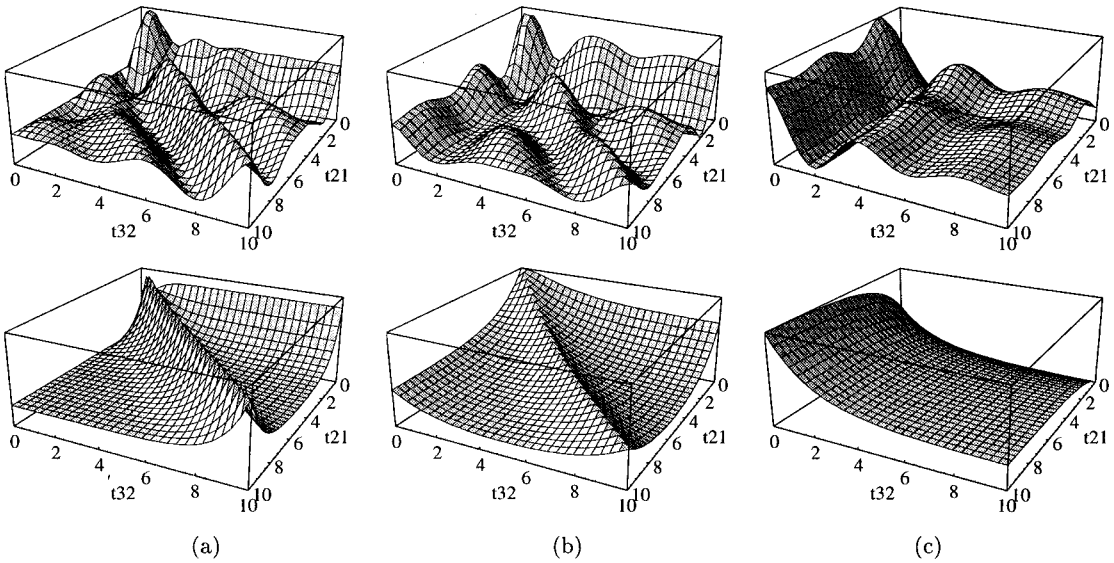

FIG. 8. Fifth-order Raman echo signals for a single inhomogeneously broadened oscillator in the underdamped (upper row) and overdamped (bottom row) limits of the inhomogeneous distribution [Eq. (5.6)]. (a)–(c) correspond to off-resonant ($\Delta\omega\sim\Omega$), near resonant, and resonant excitation, respectively. The time is given in ps.

Since the light pulses are short and do not overlap, the t_2,t_2',t_1, and t_1' integrations can be extended to $(-\infty,\infty)$. We assume that the pulse envelopes are given by a smooth function with at least one continuous time derivative. It follows from the general properties of Fourier integrals that the result of each of these four integrations vanishes at least as $(\Omega-\omega)^{-2}$. The integrals with respect to t_3,t_3' are treated similar to paths (a) and (b) and bring an additional factor of $(\Omega-\omega)^{-1}$. Consequently, S_e will scale as $(\Omega-\omega)^{-9}$.

Finally, we consider paths (c) and (d). Each involves two pairs of interactions with the field [as in (a) and (b)] and two single interactions [as in (e)]. Each pair results in the factor $(\Omega-\omega)^{-1}$, and each single interaction in $(\Omega-\omega)^{-2}$. Hence, the overall scaling of these terms $(\Omega-\omega)^{-6}$.

These arguments show that paths (a) and (b) are dominant at off resonance. The signal is then determined by $\ddot{g}_{\delta\delta}$, related to the coupling of the transition dipole to nuclear motions. When the field is tuned closer to the electronic transition frequency, the picture changes drastically. The excited-state evolution becomes essential, and paths (c), (d), and (e) start to contribute to the signal. The signal will now depend on the relative magnitude of the dipole and electronic energy coupling of electronic and nuclear degrees of freedom. If dipole coupling effects are dominant, the signal

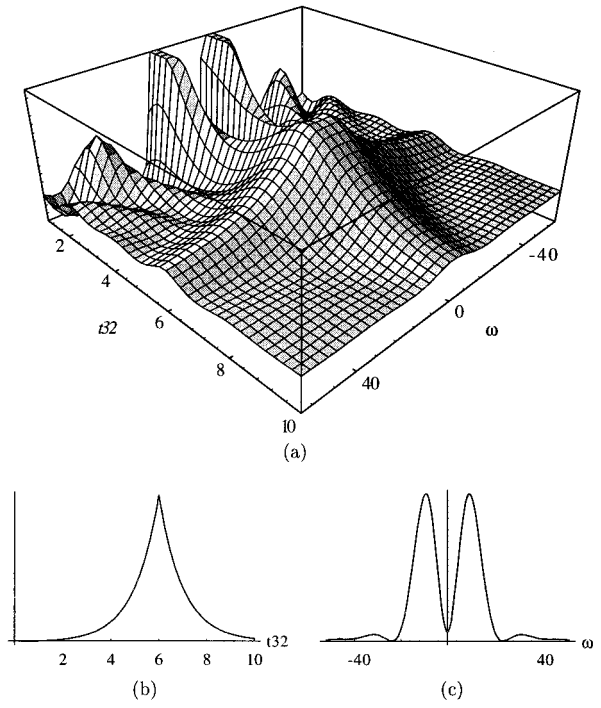

FIG. 9. (a) Wigner spectrogram of the off-resonant Raman echo [Fig. 8(a)] for the overdamped Brownian oscillator; (b) the (a) signal integrated over frequency; (c) the (a) signal integrated over time. The time units on the axes are ps, the frequency is in cm^{-1}.

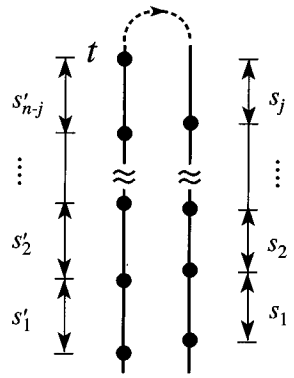

FIG. 10. The Keldysh time loop representing the two sides of the density matrix.

does not change its character as it is tuned near resonance, and its amplitude will scale as $(\Omega-\omega)^{-3}$. In the other extreme, when non-Condon effects are weak, the contribution of paths (a) and (b) in the near-resonance region becomes negligible compared with the background of the terms (c)–(e), which involve excited-state evolution. The signal then depends on the spectral density g_{dd}.

As an illustration, we calculated the Raman echo signal for a model that includes a single nuclear mode coupled to the electronic transition frequency and one mode coupled to dipole moment. We introduce inhomogeneous broadening by assuming that the frequencies of these modes are distributed around some central frequency ω_0 with half-width γ_0. The form of the distribution is taken to be of the Brownian oscillator form,[18]

$$f_{\nu\nu}(\omega)=\frac{1}{2\pi}\frac{\omega\gamma_0}{(\omega^2-\omega_0^2)^2+\omega^2\gamma_0^2},\quad \nu=d,\delta. \tag{5.6}$$

We have expanded $F^{(6)}$ to fourth order in d and δ using the expressions given in Sec. II for a single oscillator. We then averaged the result using the distribution (5.6) of the oscillator's frequency.[7] The results are presented in Fig. 8, where the Raman echo signal is calculated in the underdamped (upper row, $\gamma_0=0.6\ \text{ps}^{-1}$) and overdamped regimes (bottom row, $\gamma_0=3\ \text{ps}^{-1}$). We also used $\omega_0=1.5\ \text{ps}^{-1}$. The parameters are chosen so that near resonance the terms S_a and S_b are negligible compared with S_e. The signals (a), (b), and (c) correspond to off-resonant, intermediate, and resonant case, respectively. We see that in the former case we observe an echo (a peak at $t_{32}=t_{21}$) produced by the terms S_a and S_b. The echo gradually disappears as the electronic resonance is approached, and other contributions become dominant.

It should be noted that in the off-resonant case the Raman echo is analogous to the infrared resonant echo [Fig. 6(b)]. All the formulas remain the same, we should only replace the polarizability $\alpha(\omega,q)$ by dipole operator $M(q)$.

We next study the time- and frequency-resolved second-order infrared resonant photon echo signals. We fix the delay between the first and the second pulses t_{21} and vary the interval t_{32}. The Wigner spectrogram, defined as[39,40]

$$\mathscr{W}(t_{32},\omega)=\int_{-\infty}^{\infty}P^{(2)*}(t_{32}-\tau/2)P^{(2)}(t_{32}+\tau/2)e^{i\omega\tau}d\tau,$$

can be interpreted as the time-dependent spectrum. Integrating the Wigner spectrogram over frequencies gives the time-dependent intensity

$$\int_{-\infty}^{\infty}\mathscr{W}(t,\omega)d\omega=2\pi|P(t)|^2,$$

while integrating it over time gives the spectral distribution of the field.

$$\int_{-\infty}^{\infty}\mathscr{W}(t,\omega)dt=|P(\omega)|^2,\quad P(\omega)\equiv\int_{-\infty}^{\infty}P(t)e^{i\omega t}dt.$$

A discussion of Wigner spectrograms and their measurements is given in Refs. 39–42. The second-order polarization $P^{(2)}$ is related to three-point correlation function in Appendix A [Eq. (A12)], and the latter is given by Eq. (3.2). In Fig. 9(a) we display the Wigner spectrogram in the impulsive regime calculated using an overdamped Brownian oscillator. The parameters for the spectral density $\ddot{g}_{\mu\mu}$ are the same as for $\ddot{g}_{\delta\delta}$ in Fig. 8(a), bottom graph. In Figs. 9(b) and (c) we show the time-resolved signal (integrated over frequency) and the frequency-resolved signal (integrated over time), respectively. By comparing the time- and frequency-resolved with the integrated signals, one can clearly see the additional information contained in the former. For example, for $t_{32}\gtrsim t_{21}$ the spectrum in Fig. 9(a) shows a maximum at zero frequency, which becomes narrower as time increases. This effect is missed in the integrated signal (c), which is dominated by highly oscillating terms.

VI. DISCUSSION

We calculated the correlation functions $F^{(2)}$, $F^{(3)}$, and $F^{(4)}$ assuming that the permanent and transition dipole operators depend exponentially on nuclear coordinate [Eqs. (2.4) and (2.5)] and the coefficients μ_n and δ_n are independent of the electronic levels. Allowing μ_n and δ_n to depend on electronic levels will not affect the correlation functions $F^{(n)}_{\text{MM}}$, since it involves only the ground electronic state, but will bring additional terms to $F^{(n)}_{\text{MD}}$ and $F^{(n)}_{\text{DD}}$. As a result, the number of relevant spectral densities will increase.

The choice of the exponential form of the dipole operators [Eqs. (2.4) and (2.5)] was made for mathematical convenience in evaluating the correlation functions (2.12). The present results can, however, be used to derive expressions for an arbitrary dependence of the dipole on nuclear coordinate. This may be done using derivatives of the result with respect to the parameters δ_n and μ_n. In that sense the present results may serve as generation functions for dipole operators of arbitrary form.[6,7]

Another possible generalization of the Raman and infrared signals calculated in the previous section is to consider finite (rather than impulsive) light pulses. Let us consider four-wave mixing with nonoverlapping pulses that are short compared with nuclear motions. The external field is given by

$$E(\tau)=\frac{1}{2\pi}\sum_{j=1}^{4}\mathscr{E}_j^0\,\text{sech}[\alpha_j(\tau-t_j)]e^{i\mathbf{k}_j\mathbf{r}-i\omega_j\tau}+\text{c.c.}, \tag{6.1}$$

where the pulse j is centered at time t_j. The heterodyne-detected signal in the direction $\mathbf{k}_s=\mathbf{k}_1-\mathbf{k}_2+\mathbf{k}_3$ is

$$S(\omega_1,\omega_2,\omega_3,\omega_4)=\frac{2}{\hbar^3}\,\mathrm{Re}\int\!\!\int\!\!\int\!\!\int_{-\infty}^{\infty} d\tau_1 d\tau_2 d\tau_3 d\tau_4 \mathscr{E}_1(\tau_1)\mathscr{E}_2^*(\tau_2)\mathscr{E}_3(\tau_3)\mathscr{E}_4^*(\tau_4)e^{-i\omega_1\tau_1+i\omega_2\tau_2-i\omega_3\tau_3+i\omega_4\tau_4}$$
$$\times[F_{DD}^{(4)}(\tau_1,\tau_2,\tau_3,\tau_4)-F_{DD}^{(4)}(\tau_1,\tau_2,\tau_4,\tau_3)-F_{DD}^{(4)}(\tau_1,\tau_3,\tau_4,\tau_2)-F_{DD}^{(4)}(\tau_2,\tau_3,\tau_4,\tau_1)],$$

where the four-point correlation function $F_{DD}^{(4)}$ is given by Eq. (B4). We factorize the fast-oscillating part of the four-point correlation function as in Eq. (4.6), and assuming that nuclear motions are slow, we can take the slowly-varying function Φ out of the integral, setting in it $\tau_j=t_j$. We then have

$$S(\omega_1,\omega_2,\omega_3,\omega_4)=-\frac{1}{\hbar^3}\,\mathrm{Re}[I_1^-(\omega_1)I_2^-(\omega_2)I_3^+(\omega_3)I_4^+(\omega_4)\Phi(t_1,t_2,t_3,t_4)-I_1^-(\omega_1)I_2^-(\omega_2)I_3^-(\omega_3)I_4^-(\omega_4)\Phi(t_1,t_2,t_4,t_3)$$
$$-I_1^-(\omega_1)I_2^-(\omega_2)I_3^-(\omega_3)I_4^-(\omega_4)\Phi(t_1,t_3,t_4,t_2)-I_1^+(\omega_1)I_2^+(\omega_2)I_3^-(\omega_3)I_4^-(\omega_4)\Phi(t_2,t_3,t_4,t_1)], \qquad (6.2)$$

where

$$I_j^-(\omega_j)=\frac{\mathscr{E}_j^0}{\alpha_j}\mathrm{sech}[\pi(\omega_j-\Omega)/(2\alpha_j)], \qquad (6.3)$$

$$I_j^+(\omega_j)=\frac{\mathscr{E}_j^0}{\alpha_j}\mathrm{sech}[\pi(\omega_j+\Omega)/(2\alpha_j)]. \qquad (6.4)$$

If the field frequency is close to resonance, $\omega_j\approx\Omega$, then $I_j^-(\omega_j)\gg I_j^+(\omega_j)$; this means that the terms in Eq. (6.2) that involve the counter-rotating factors $I_j^+(\omega_j)$ can be neglected. When the field frequency ω_j is tuned off the resonance frequency Ω, the factors $I_j^-(\omega_j)$ vanish exponentially. Note that this scaling depends on the pulse shape. In the fifth-order Raman signals calculated in the preceding section we assumed that the pulse envelopes have only one continuous time derivative. In that case, each convolution with the field results in an additional $(\omega_j-\Omega)^{-2}$ factor coming from $I_j^-(\omega_j)$. If the envelope has a continuous nth derivative, the factors $I_j^-(\omega_j)$ scale as $(\omega_j-\Omega)^{-n+1}$. Finally, if the envelopes are given by infinitely differentiable functions, the scaling becomes much more rapid (e.g., exponential for sech pulses). The asymptotic off-resonant scaling of four-wave mixing signals is thus very sensitive to the pulse envelopes. Smooth envelopes result in a fast (e.g., exponential) scaling with frequency, whereas less smooth envelopes will show a more gradual scaling, reflecting their broader spectral distribution.

ACKNOWLEDGMENTS

The support of the National Science Foundation and the Air Force Office of Scientific Research is gratefully acknowledged.

APPENDIX A: PARTIALLY TIME ORDERED EXPRESSIONS FOR RESPONSE FUNCTIONS

Optical signals are related to the induced polarization by the external radiation field

$$P(t)=\mathrm{Tr}[V\rho(t)]. \qquad (A1)$$

Expanding the density matrix $\rho(t)$ in powers of the electric field, we obtain for the nth-order contribution

$$P^{(n)}(t)=\mathrm{Tr}[V\rho^{(n)}(t)]. \qquad (A2)$$

The density matrix can be represented in the form

$$\rho(t)=\sum_a P(a)|\psi_a(t)\rangle\langle\psi_a(t)|, \qquad (A3)$$

where $|\psi_a\rangle$ are the eigenvalues of the molecular Hamiltonian. Hence,

$$\rho^{(n)}(t)=\sum_a P(a)\sum_{j=0}^{n}|\psi_a^{(n-j)}(t)\rangle\langle\psi_a^j(t)|, \qquad (A4)$$

where

$$|\psi_a^{(j)}(t)\rangle=\left(\frac{i}{\hbar}\right)^j\int_0^\infty ds_j\int_0^\infty ds_{j-1}\cdots\int_0^\infty ds_1 E(\mathbf{r},t-s_j)\cdots E(\mathbf{r},t-s_j-\cdots-s_1)G(s_j)VG(s_{j-1})\cdots G(s_1)|\psi_a(-\infty)\rangle, \qquad (A5)$$

and Eq. (A1) becomes

$$P^{(n)}(t)=\left(\frac{i}{\hbar}\right)^n\sum_a P(a)\sum_{j=0}^{n}\int_0^\infty ds_1\cdots\int_0^\infty ds_{n-j}\int_0^\infty ds_1'\cdots\int_0^\infty ds_j' \qquad (A6)$$
$$\times E(\mathbf{r},t-s_{n-j})\cdots E(\mathbf{r},t-s_{n-j}-\cdots-s_1)E(\mathbf{r},t-s_j')\cdots E(\mathbf{r},t-s_j'-\ldots-s_1')$$
$$\times\mathrm{Tr}[VG(s_{n-j})V\cdots VG(s_1)|\psi_a(-\infty)\rangle\langle\psi_a(-\infty)|G^\dagger(s_1')V\cdots VG^\dagger(s_j')]. \qquad (A7)$$

In this expression the ket and the bra time intervals $s_1,\ldots,s_{n-j}$ and $s_1',\ldots,s_j'$, respectively, are independent. We next use the cyclic invariance of the trace and move all the operators that act on the vector $\langle\psi_a(-\infty)|$ to the left. This results in

$$P^{(n)}(t)=\left(\frac{i}{\hbar}\right)^n\sum_j\int_0^\infty ds_1\cdots\int_0^\infty ds_{n-j}\int_0^\infty ds_1'\cdots\int_0^\infty ds_j' E(\mathbf{r},t-s_j)\cdots E(\mathbf{r},t-s_{n-j}-\cdots-s_1)$$
$$\times E(\mathbf{r},t-s_{n-j}')\cdots E(\mathbf{r},t-s_j'-\cdots-s_1')\mathrm{Tr}[G^\dagger(s_1')V\cdots VG(s_j')VG(s_{n-j})V\cdots VG(s_1)\rho(-\infty)], \tag{A8}$$

where

$$\rho(-\infty)=\sum_a P(a)|\psi_a(-\infty)\rangle\langle\psi_a(-\infty)|.$$

Defining the time-dependent dipole operators $V(t)\equiv G^\dagger(t)VG(t)$ and recalling that $\mathrm{Tr}(A,\rho)=\langle A\rangle$, we finally obtain

$$P^{(n)}(t)=\left(\frac{i}{\hbar}\right)^n\sum_j\int_0^\infty ds_1\cdots\int_0^\infty ds_{n-j}\int_0^\infty ds_1'\cdots\int_0^\infty ds_j'$$
$$\times\langle V(t-s_j'-\cdots-s_1')\cdots V(t-s_j')V(t)V(t-s_{n-j})\cdots V(t-s_{n-j}-\cdots-s_1)\rangle$$
$$\times E(\mathbf{r},t-s_{n-j})\cdots E(\mathbf{r},t-s_{n-j}-\cdots-s_1)E(\mathbf{r},t-s_j')\cdots E(\mathbf{r},t-s_j'-\cdots-s_1'). \tag{A9}$$

The calculation of the dipole correlation function is illustrated by Fig. 10. In contrast to the Liouville-space representation, we consider the evolution of the bra and ket of the density matrix independently and do not maintain time-ordering of all interactions with the external field; only the interactions on the bra and ket separately are time-ordered. The Liouville-space representation provides a deep physical insight and is particularly suitable for calculating time-domain response with short non-overlapping pulses, since it follows the fully time-ordered evolution of the density matrix. In the case of overlapping pulses, keeping the time order separately for bra and ket (partial time-ordering) may allow us to significantly reduce the number of terms necessary to calculate the signal.[40] This bookkeeping corresponds to the wave function representation (see Ref. 18) and is similar to the Keldysh-Schwinger time loop technique.[35–37] The only difference is that in the latter, the two sides of the path diagram are connected at infinite time (which is convenient for a frequency-domain analysis), whereas we close the loop at the time of last interaction with the field. We move along the left side of the path diagram and then return to the starting point along the right side. In doing so we can naturally write all the dipole operators in a properly time-ordered form. We define the n-point dipole correlation function

$$F^{(n)}(\tau_1,\tau_2,\ldots,\tau_n)\equiv\langle V(\tau_1)V(\tau_2)\cdots V(\tau_n)\rangle, \tag{A10}$$

and all correlation functions in Eq. (A9) can be expressed in terms of this function by a specific choice of time arguments.

We present below the explicit expressions for the first, second, and third order response

$$P^{(1)}(t)=\frac{i}{\hbar}\int_0^\infty ds F^{(2)}(t,t-s)E(\mathbf{r},t-s)+\text{c.c.}, \tag{A11}$$

$$P^{(2)}(t)=\left(\frac{i}{\hbar}\right)^2\iint_0^\infty ds_1ds_2F^{(3)}(t,t-s_2,t-s_1-s_2)E(\mathbf{r},t-s_1-s_2)E(\mathbf{r},t-s_2)$$
$$+\frac{1}{2}\left(\frac{i}{\hbar}\right)^2\iint_0^\infty ds_1ds_1'F^{(3)}(t-s_1,t,t-s_1')E(\mathbf{r},t-s_1)E(\mathbf{r},t-s_1')+\text{c.c.}, \tag{A12}$$

$$P^{(3)}(t)=\left(\frac{i}{\hbar}\right)^3\iiint_0^\infty ds_1ds_2ds_3F^{(4)}(t,t-s_3,t-s_3-s_2,t-s_3-s_2-s_1)E(\mathbf{r},t-s_3-s_2-s_1)E(\mathbf{r},t-s_3-s_2)E(\mathbf{r},t-s_3)$$
$$+\left(\frac{i}{\hbar}\right)^2\iiint_0^\infty ds_1ds_2ds_1'F^{(4)}(t-s_1',t,t-s_2,t-s_2-s_1)E(\mathbf{r},t-s_2-s_1)E(\mathbf{r},t-s_2)E(\mathbf{r},t-s_1')+\text{c.c.}, \tag{A13}$$

The calculation of the nth-order nonlinear response is thus reduced to the computation of the $(n+1)$-point dipole correlation function $F^{(n+1)}(\tau_1,\ldots,\tau_{n+1})$.

TABLE II. The parameters corresponding to six terms of the sum $F^{(4)}_{\rm MD}$ [the diagrams (a)–(f) in Fig. 2].

k	Path	$\tau_{\rm DD}$	$\tau_{\rm MM}$	$\tau^{(1)}_{\rm MD}$	$\tau^{(2)}_{\rm MD}$	$\tau^{(3)}_{\rm MD}$	$\tau^{(4)}_{\rm MD}$	$\varepsilon^k_1,\varepsilon^k_2$	ε^k_3	ε^k_4	M^2_k
1	(a)	τ_{43}	τ_{21}	τ_{42}	τ_{41}	τ_{32}	τ_{31}	1	-1	-1	M^2_0
2	(b)	τ_{42}	τ_{31}	τ_{32}	τ_{41}	τ_{21}	τ_{43}	1	-1	1	M_0M_j
3	(c)	τ_{41}	τ_{32}	τ_{21}	τ_{42}	τ_{31}	τ_{43}	1	1	1	M^2_j
4	(d)	τ_{21}	τ_{43}	τ_{41}	τ_{31}	τ_{32}	τ_{42}	1	-1	-1	M^2_0
5	(e)	τ_{31}	τ_{42}	τ_{21}	τ_{32}	τ_{43}	τ_{41}	1	-1	1	M_0M_j
6	(f)	τ_{32}	τ_{41}	τ_{43}	τ_{31}	τ_{21}	τ_{43}	1	-1	-1	M^2_0

APPENDIX B: FOUR-POINT CORRELATION FUNCTIONS FOR THE THIRD-ORDER RESPONSE

We present here the four-point correlation functions calculated for the model introduced in Sec. II.

$$F^{(4)}(\tau_1,\tau_2,\tau_3,\tau_4)=F^{(4)}_{\rm MM}(\tau_1,\tau_2,\tau_3,\tau_4)+F^{(4)}_{\rm MD}(\tau_1,\tau_2,\tau_3,\tau_4)+F^{(4)}_{\rm DD}(\tau_1,\tau_2,\tau_3,\tau_4)+F^{(4)}_{\rm DD'}(\tau_1,\tau_2,\tau_3,\tau_4), \tag{B1}$$

$$F^{(4)}_{\rm MM}(\tau_1,\tau_2,\tau_3,\tau_4)=M_0^4\,\exp\{2\ddot g_{\mu\mu}(0)+\ddot g_{\mu\mu}(\tau_{21})+\ddot g_{\mu\mu}(\tau_{32})+\ddot g_{\mu\mu}(\tau_{43})+\ddot g_{\mu\mu}(\tau_{31})+\ddot g_{\mu\mu}(\tau_{42})+\ddot g_{\mu\mu}(\tau_{41})\}, \tag{B2}$$

$$\begin{aligned}F^{(4)}_{\rm MD}(\tau_1,\tau_2,\tau_3,\tau_4)=\sum_{k=1}^{6}\sum_j M_k^2D_{j0}^2\,\exp\Big\{&-i\Omega\tau_{\rm DD}+\ddot g_{\mu\mu}(0)+\ddot g_{\mu\mu}(\tau_{\rm MM})+\ddot g_{\delta\delta}(0)+\ddot g_{\delta\delta}(\tau_{\rm DD})-g_{d_jd_j}(\tau_{\rm DD})\\&+2i\dot g_{\delta d_j}(\tau_{\rm DD})+i\sum_{n=1}^{4}\dot g_{\delta\mu}(\tau^{(n)}_{\rm MD})+i\sum_{n=1}^{4}\varepsilon^k_n\dot g_{d_j\mu}(\tau^{(n)}_{\rm MD})\Big\}\end{aligned} \tag{B3}$$

$$\begin{aligned}F^{(4)}_{\rm DD}(\tau_1,\tau_2,\tau_3,\tau_4)=\sum_j D^4_{j,0}\,\exp\{&-i\Omega_j(\tau_{43}+\tau_{21})+2i[\dot g_{\delta d_j}(\tau_{21})-\dot g_{\delta d_j}(\tau_{32})+\dot g_{\delta d_j}(\tau_{43})+\dot g_{\delta d_j}(\tau_{41})]\\&+2\ddot g_{\delta\delta}(0)+\ddot g_{\delta\delta}(\tau_{21})+\ddot g_{\delta\delta}(\tau_{32})+\ddot g_{\delta\delta}(\tau_{43})+\ddot g_{\delta\delta}(\tau_{31})+\ddot g_{\delta\delta}(\tau_{42})+\ddot g_{\delta\delta}(\tau_{41})\\&-g_{d_jd_j}(\tau_{21})-g_{d_jd_j}(\tau_{32})-g_{d_jd_j}(\tau_{43})+g_{d_jd_j}(\tau_{31})+g_{d_jd_j}(\tau_{42})-g_{d_jd_j}(\tau_{41})\},\end{aligned} \tag{B4}$$

$$\begin{aligned}F^{(4)}_{\rm DD'}(\tau_1,\tau_2,\tau_3,\tau_4)=\sum_{j,i} D^2_{ij}D^2_{j0}\,\exp\{&-i\Omega_j(\tau_{43}+\tau_{21})-i\Omega_i(\tau_{32})+2i\dot g_{\delta d_j}(\tau_{21})-i\dot g_{\delta d_i}(\tau_{21})-2i\dot g_{\delta d_j}(\tau_{32})+2i\dot g_{\delta d_i}(\tau_{32})\\&+2i\dot g_{\delta d_j}(\tau_{43})-i\dot g_{\delta d_i}(\tau_{43})+i\dot g_{\delta d_i}(\tau_{31})+i\dot g_{\delta d_i}(\tau_{42})+2i\dot g_{\delta d_j}(\tau_{41})+2\ddot g_{\delta\delta}(0)+\ddot g_{\delta\delta}(\tau_{21})+\ddot g_{\delta\delta}(\tau_{32})\\&+\ddot g_{\delta\delta}(\tau_{43})+\ddot g_{\delta\delta}(\tau_{31})+\ddot g_{\delta\delta}(\tau_{42})+\ddot g_{\delta\delta}(\tau_{41})-g_{d_jd_j}(\tau_{21})+g_{d_jd_i}(\tau_{21})-g_{d_jd_j}(\tau_{32})+2g_{d_jd_i}(\tau_{32})\\&-g_{d_id_i}(\tau_{32})-g_{d_jd_j}(\tau_{43})+g_{d_jd_i}(\tau_{43})+g_{d_jd_j}(\tau_{31})-g_{d_jd_i}(\tau_{31})+g_{d_jd_j}(\tau_{42})-g_{d_jd_i}(\tau_{42})-g_{d_jd_j}(\tau_{41})\}.\end{aligned} \tag{B5}$$

Here, $\tau_{ij}\equiv\tau_i-\tau_j$, $i,j=1,\ldots,4$, and the variables $\tau_{\rm DD}$, $\tau_{\rm MM}$, and $\tau_{\rm MD}$ in Eq. (B3) denote time intervals between two D-interactions, two M-interactions, and a D- and an M-interactions, respectively. The sum over k in Eq. (B3) runs over six choices of the interval $\tau_{\rm DD}$; these terms are given in Figs. 2(a)–2(f). The subscripts k of M_k indicate whether the ground or excited state permanent dipole operator is involved. All relevant time intervals and parameters are listed in Table II.

APPENDIX C: THE HETERODYNE-DETECTED TRANSIENT GRATING (HDTG) SIGNAL

To derive a correlation-function expression for the HDTG signal, we start with Eq. (4.5). Expressing the polarization through four-point correlation function, we obtain

$$\begin{aligned}S(\omega_1,\omega_2;\tau_0)=\frac{2}{\hbar^3}\,{\rm Re}\int_{-\infty}^{\infty}dt_1\int_0^{\infty}d\tau_1\int_{-\infty}^{\infty}dt_2\int_0^{\infty}d\tau_2\mathscr{E}_2(t_2-\tau_0)\mathscr{E}_2^*(t_2-\tau_0-\tau_2)e^{-i\omega_2\tau_2+i\varphi}\\\times[\mathscr{E}_1(t_1)\mathscr{E}_1^*(t_1-\tau_1)e^{-i\omega_1\tau_1}+\mathscr{E}_1^*(t_1)\mathscr{E}_1(t_1-\tau_1)e^{i\omega_1\tau_1}]\{F^{(4)}_{\rm DD}(t_1-\tau_1,t_1,t_2-\tau_2,t_2)\\-F^{(4)}_{\rm DD}(t_1-\tau_1,t_1,t_2,t_2-\tau_2)-F^{(4)}_{\rm DD}(t_1,t_2-\tau_2,t_2,t_1-\tau_1)+F^{(4)}_{\rm DD}(t_1,t_2,t_2-\tau_2,t_1-\tau_1)-{\rm c.c.}\}.\end{aligned} \tag{C1}$$

We next factorize the four-point correlation function $F^{(4)}_{\rm DD}$ [Eq. (B4)] into two parts: the fast-oscillating term $\exp\{-i\Omega(t_4-t_3+t_2-t_1)\}$ and a slowly-varying function $\Phi(t_1,t_2,t_3,t_4)$

$$F^{(4)}_{\mathrm{DD}}(t_1,t_2,t_3,t_4)\equiv D^4 e^{-i\Omega(t_4-t_3+t_2-t_1)}\Phi(t_1,t_2,t_3,t_4). \tag{C2}$$

Using the function Φ defined in Eq. (C2), we can recast Eq. (C1) in the form

$$\begin{aligned}S(\omega_1,\omega_2;\tau_0)=\frac{2}{\hbar^2}\,\mathrm{Re}\int_{-\infty}^{\infty}dt_1\int_0^{\infty}d\tau_1\int_{-\infty}^{\infty}dt_2\int_0^{\infty}d\tau_2\,\mathscr{E}_2(t_2-\tau_0)\mathscr{E}_2^*(t_2-\tau_0-\tau_2)e^{-i\omega_2\tau_2+i\varphi}\\ \times[\mathscr{E}_1(t_1)\mathscr{E}_1^*(t_1-\tau_1)e^{-i\omega_1\tau_1}+\mathscr{E}_1^*(t_1)\mathscr{E}_1(t_1-\tau_1)e^{i\omega_1\tau_1}]\\ \times\{e^{-i\Omega\tau_2}e^{-i\Omega\tau_1}\Phi(t_1-\tau_1,t_1,t_2-\tau_2,t_2)-e^{i\Omega\tau_2}e^{-i\Omega\tau_1}\Phi(t_1-\tau_1,t_1,t_2,t_2-\tau_2)\\ -e^{-i\Omega\tau_2}e^{-i\Omega\tau_1}\Phi(t_1,t_2-\tau_2,t_2,t_1-\tau_1)+e^{i\Omega\tau_2}e^{-i\Omega\tau_1}\Phi(t_1,t_2,t_2-\tau_2,t_1-\tau_1)-\mathrm{c.c.}\}.\end{aligned} \tag{C3}$$

We further assume the snapshot limit[38], in which (i) the durations of the pulses are short compared with the nuclear dynamics and (ii) the pulses are long compared with the electronic dephasing time. The first assumption allows us to neglect the variation of the function Φ on the timescale of the pulse duration and put in it $t_2=\tau_0$ and $t_1=0$. The second assumption yields

$$\int_{-\infty}^{\infty}\mathscr{E}_1(t_1)\mathscr{E}_1^*(t_1-\tau_1)dt_1\approx\int_{-\infty}^{\infty}|\mathscr{E}_1(t_1)|^2dt_1\equiv E_1,$$

$$\int_{-\infty}^{\infty}\mathscr{E}_2^*(t_2-\tau_0)\mathscr{E}_2(t_2-\tau_0-\tau_2)dt_2\approx\int_{-\infty}^{\infty}|\mathscr{E}_2(t_2-\tau_0)|^2dt_2\equiv E_2.$$

Equation (C3) then assumes the form

$$\begin{aligned}S(\omega_1,\omega_2;\tau_0)=\frac{4}{\hbar^2}E_1E_2\,\mathrm{Re}\iint_0^{\infty}d\tau_1d\tau_2\,\cos(\omega_1\tau_1)e^{-i\omega_2\tau_2+i\varphi}\{e^{-i\Omega\tau_2}e^{-i\Omega\tau_1}\Phi(-\tau_1,0,\tau_{02},\tau_0)\\ -e^{i\Omega\tau_2}e^{-i\Omega\tau_1}\Phi(-\tau_1,0,\tau_0,\tau_{02})-e^{-i\Omega\tau_2}e^{i\Omega\tau_1}\Phi(0,\tau_{02},\tau_0,-\tau_1)+e^{i\Omega\tau_2}e^{i\Omega\tau_1}\Phi(0,\tau_0,\tau_{02},-\tau_1)-\mathrm{c.c.}\},\end{aligned} \tag{C4}$$

where we used the notation $\tau_{02}\equiv\tau_0-\tau_2$. This equation can be further simplified by invoking the rotating-wave approximation, resulting in Eq. (4.7).

[1] D. McMorrow and W. T. Lotshaw, J. Chem. Phys. **95**, 10395 (1991).
[2] M. Cho, M. Du, N. F. Scherer, G. R. Fleming, and S. Mukamel, J. Chem. Phys. **99**, 2410 (1993).
[3] A. Waldman, U. Banin, E. Rabani, and S. Ruhman, J. Chem. Phys. **96**, 10842 (1992); S. Ruhman and K. A. Nelson, *ibid.* **94**, 859 (1991).
[4] J. T. Fourkas and M. D. Fayer, Acc. Chem. Research, **25**, 227 (1992); J. T. Fourkas, R. Trebino, and M. D. Fayer, J. Chem. Phys. **97**, 69 (1992).
[5] R. F. Loring and S. Mukamel, J. Chem. Phys. **83**, 2119 (1985).
[6] Y. Tanimura and S. Mukamel, J. Chem. Phys. **99**, 9496 (1993).
[7] V. Khidekel and S. Mukamel, Chem. Phys. Lett. **240**, 304 (1995).
[8] R. R. Ernst, G. Bodenhausen, and A. Wokaun, *Principles of Nuclear Magnetic Resonance in One and Two Dimensions* (Clarendon, Oxford, 1987).
[9] N. A. Kurnit, I. D. Albella, S. R. Hartmann, Phys. Rev. Lett. **13**, 567 (1964).
[10] E. T. J. Nibbering, D. A. Wiersma, and K. Duppen, Phys. Rev. Lett. **66**, 2464 (1991).
[11] C. J. Barden and C. V. Shank, Chem Phys. Lett. **226**, 310 (1994).
[12] Thomas Steffen and Koos Duppen, Phys. Rev. Lett. **76**, 1224 (1996).
[13] M. Cho, G. R. Fleming, and S. Mukamel, J. Chem. Phys. **98**, 5314 (1993).
[14] M. Cho, M. Du, N. F. Scherer, G. R. Fleming, and S. Mukamel, J. Chem. Phys. **99**, 2410 (1993).
[15] *Persistent Spectral Hole Burning. Science and Applications*, edited by W. E. Moerner (Springer, Berlin, 1988).
[16] D. Haarer, R. J. Silbey, Phys. Today **43**, 58 (1990).
[17] A. A. Villaeys, J. C. Vallet, H. Ma, and S. H. Lin, Phys. Rev. A **16**, 5959 (1992).
[18] S. Mukamel, *Principles of Nonlinear Optical Spectroscopy* (Oxford University Press, New York, 1995).
[19] T. Joo, Y. Jia, J.-Y. Yu, M. J. Lang, and G. R. Fleming, J. Chem. Phys. **104**, 6089 (1996).
[20] D. Vanden Bout, L. J. Muller, and M. Berg, Phys. Rev. Lett. **67**, 3700 (1991).
[21] K. Tominaga and K. Yoshihara, J. Chem. Phys. **104**, 1159 (1996).
[22] K. Tominaga and K. Yoshihara, J. Chem. Phys. (in press).
[23] M. Cho, G. R. Fleming, and S. Mukamel, J. Chem. Phys. **98**, 5314 (1992).
[24] Y. Tanimura and S. Mukamel, J. Opt. Soc. Am. B **10**, 2263 (1993).
[25] D.-Y Zang, Y. Q. Shi, F. F. So, S. R. Forrest, and W. H Steier, Appl. Phys. Lett. **58**, 562 (1991).
[26] Y. K. Shin, B. S. Brunschwig, and N. Sutin, J. Phys. Chem. **100**, 8157 (1996).
[27] A. Tokmakoff, A. S. Kwok, R. S. Urdahl, R. S. Francis, and M. D. Fayer, Chem. Phys. Lett. **234**, 289 (1995).
[28] T. Keyes, J. Phys. Chem. **103**, 9810 (1995).
[29] M. Cho, G. Fleming, S. Saito, I. Ohmine, and R. Stratt, J. Chem. Phys. **100**, 6672 (1994).
[30] S. Schvaneveldt and R. Loring, J. Chem. Phys. **102**, 2326 (1995).
[31] B. M. Ladanyi and R. M. Stratt, J. Phys. Chem. **100**, 1266 (1996).
[32] A. O. Caldeira and A. J. Leggett, Phys. Status Solidi A **121**, 587 (1983).
[33] R. J. Glauber, Phys. Rev. **131**, 2766 (1963).
[34] J. R. Klauder and Bo-Stute Skagerstam, *Coherent States - Applications in Physics and Mathematical Physics* (World Scientific, Singapore, 1985).
[35] L. V. Keldysh, Zh. Éksp. Teor. Fiz. **47**, 1515 (1964) [Soviet Phys. JETP **20**, 1018 (1965)].
[36] E. M. Lifshitz and L. P. Pitaevsky, *Physical Kinetics* (Pergamon, Oxford, 1981).
[37] J. Schwinger, J. Math. Phys. **2**, 407 (1961).
[38] Y. J. Yan and S. Mukamel, J. Chem. Phys. **94**, 997 (1990).
[39] S. Mukamel, C. Ciordas-Ciurdariu, and V. Khidekel, IEEE J. Quantum Electr. **32**, 1278 (1996).
[40] S. Mukamel, C. Ciordas-Ciurdariu, and V. Khidekel, Adv. Chem. Phys. (in press).
[41] L. Cohen, Proc. IEEE, **77**, 941 (1989).
[42] K. H. Brenner and K. Wodkiewicz, Opt. Commun. **43**, 103 (1982).